Science Advances
AAAS

Supplementary Materials for

Conformational changes in the yeast mitochondrial ABC transporter Atm1 during the transport cycle

Thomas L. Ellinghaus, Thomas Marcellino, Vasundara Srinivasan,
Roland Lill*, Werner Kühlbrandt*

*Corresponding author. Email: werner.kuehlbrandt@biophys.mpg.de (W.K.); lill@staff.uni-marburg.de (R.L.)

Published 22 December 2021, *Sci. Adv.* **7**, eabk2392 (2021)
DOI: 10.1126/sciadv.abk2392

This PDF file includes:

Supplementary figures

Figure S1

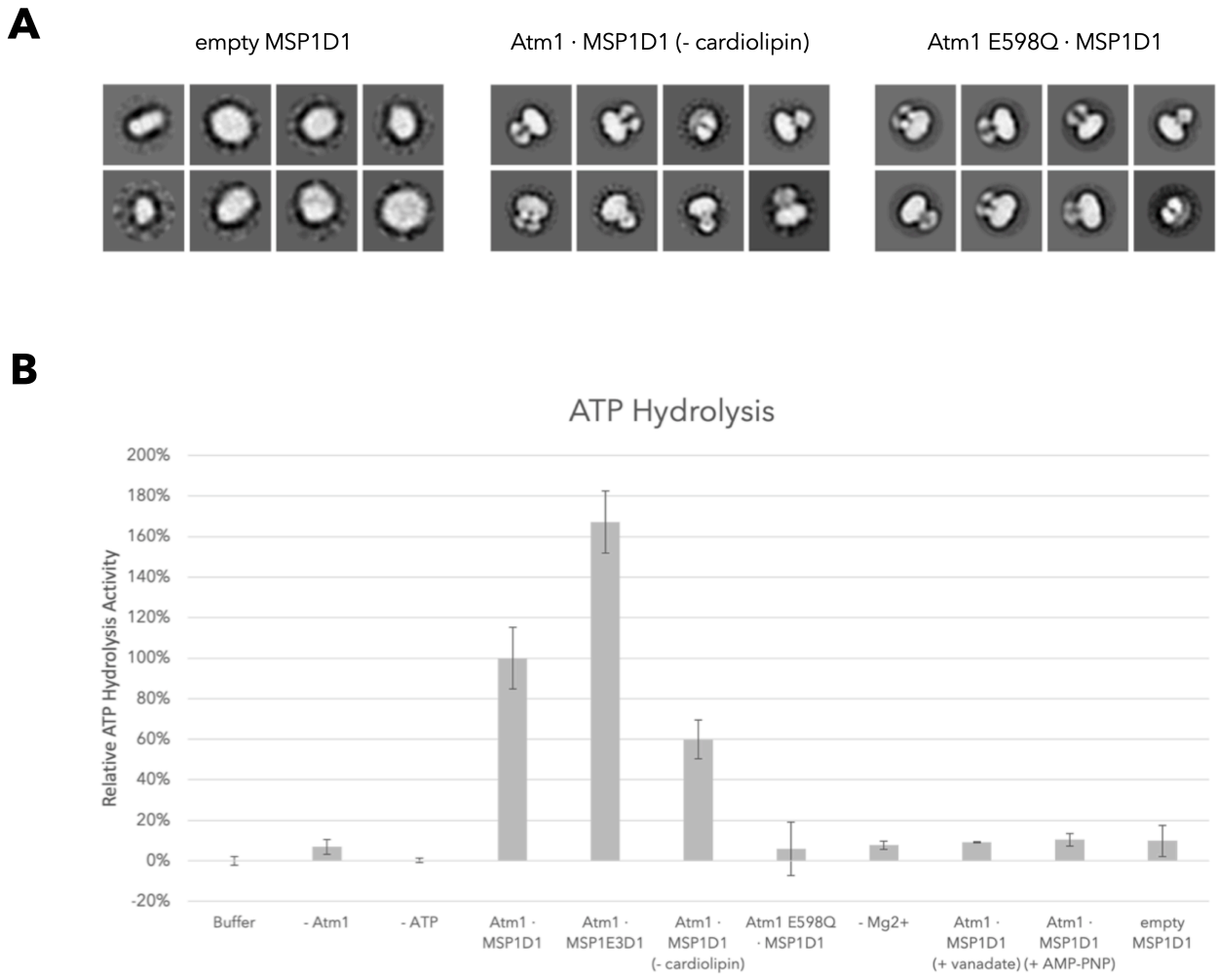

Figure S1: **ATP hydrolysis activity of Atm1 in MSP lipid nanodiscs.** (**A**) Representative negative-stain EM 2D class averages of empty MSP1D1 nanodisc, cardiolipin-free variant, and Atm1 E598Q in MSP1D1 nanodiscs as used in the ATP hydrolysis assay. (**B**) Specific ATPase activities are presented relative to that of wild-type Atm1 in MSP1D1 nanodiscs (1.1 μmol free phosphate per minute and mg Atm1). Control samples without Atm1, ATP, or $MgCl_2$, and empty nanodiscs have background activity. Error bars denote standard errors of triplicates.

Figure S2

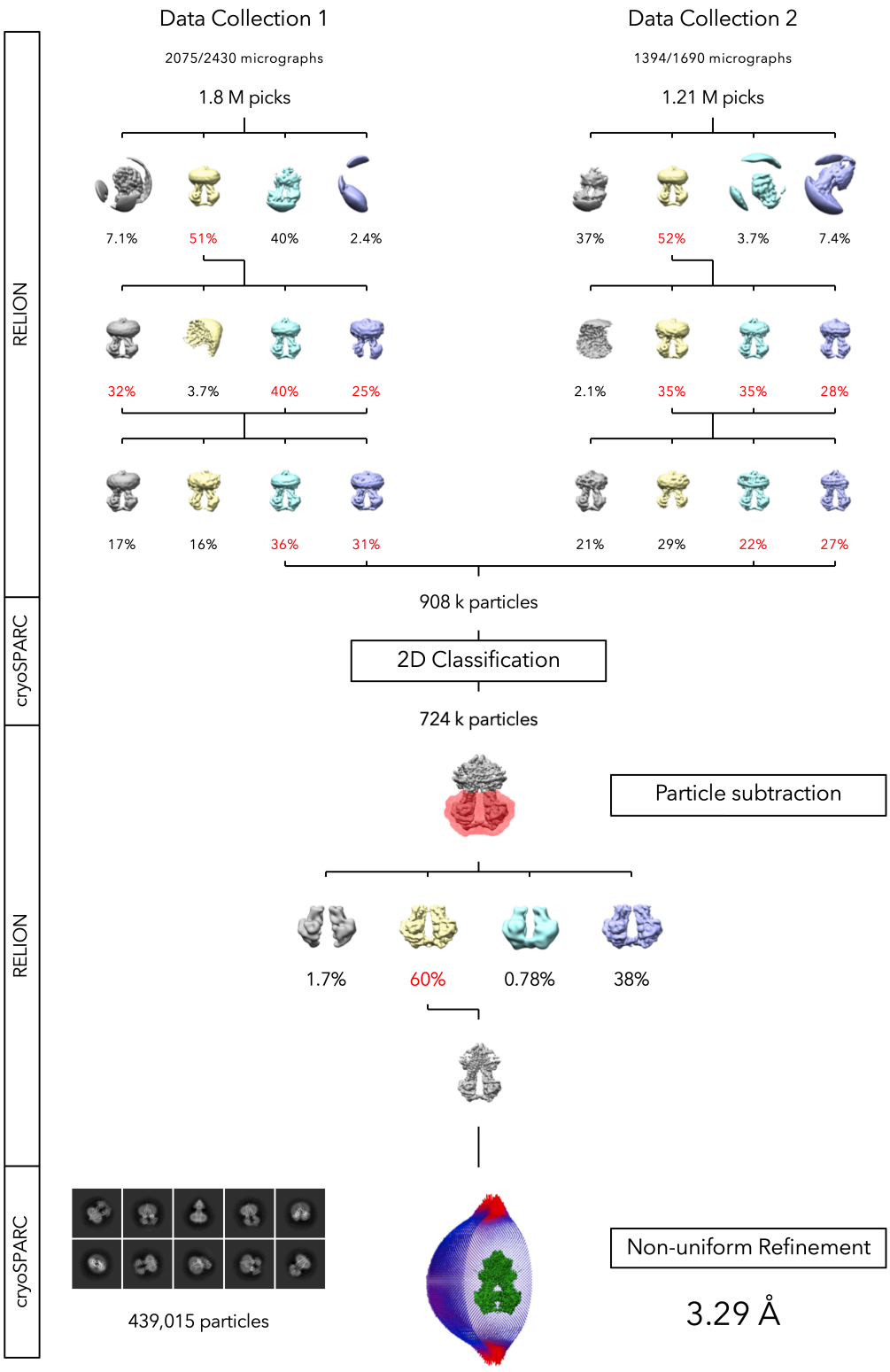

Figure S2: **Cryo-EM data processing pipeline for nucleotide-free yeast Atm1 in MSP1D1 nanodiscs.** See Methods.

Figure S3

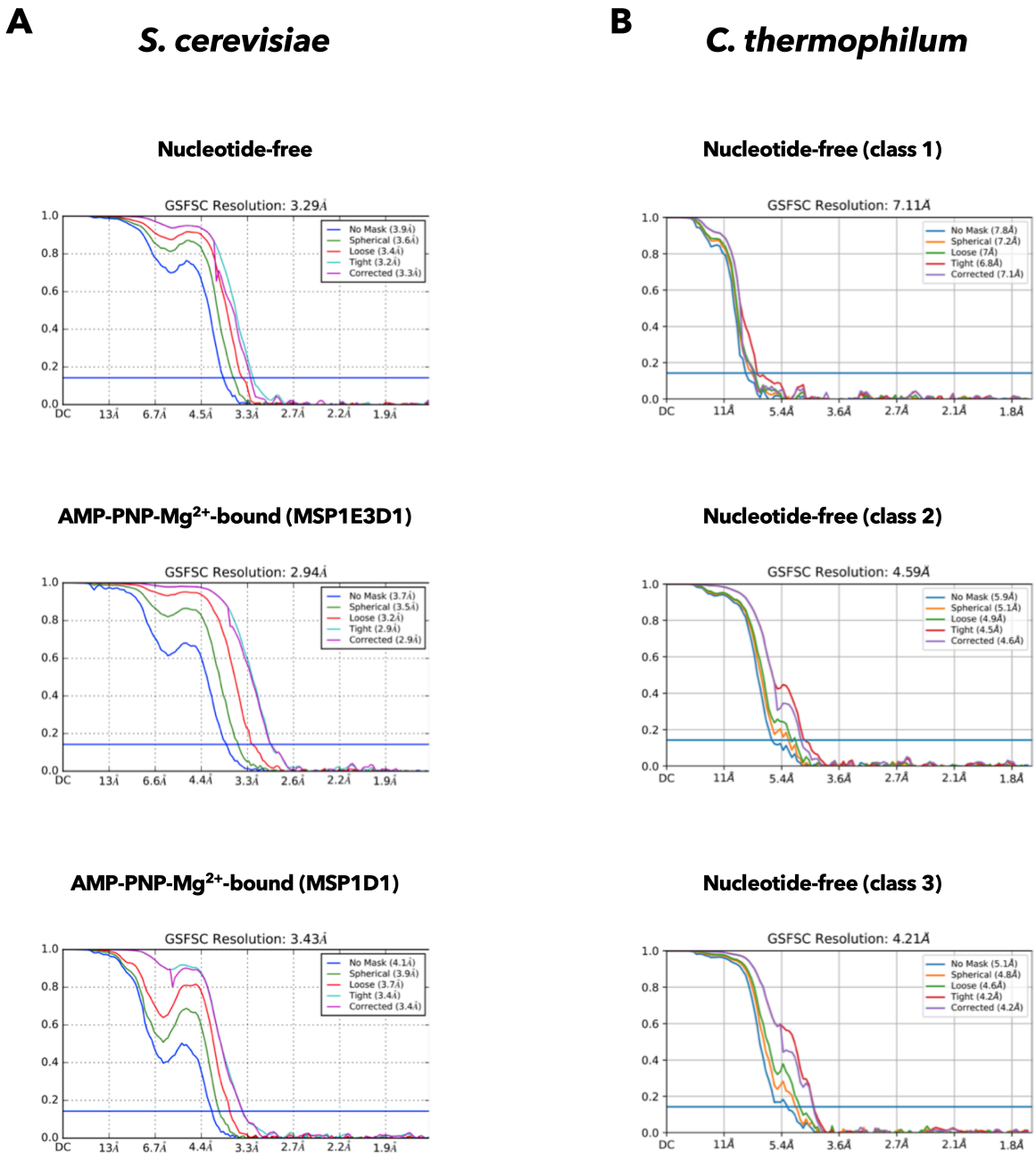

Figure S3: **Fourier shell correlation (FSC) curves.** FSC curves are shown for Non-uniform refinements of ScAtm1 (**A**; cryoSPARC v2.15.0) or CtAtm1 (**B**; cryoSPARC v.3.0.1). (**A**) *Top:* Nucleotide-free apo-state. *Middle:* AMP-PNP-Mg^{2+}-bound occluded state in MSP1E3D1 lipid nanodiscs. *Below:* AMP-PNP-Mg^{2+}-bound occluded state in MSP1D1 lipid nanodiscs. (**B**) Refinement maps of classes 1 (top), 2 (middle) and 3 (below) of nucleotide-free CtAtm1.

Figure S4

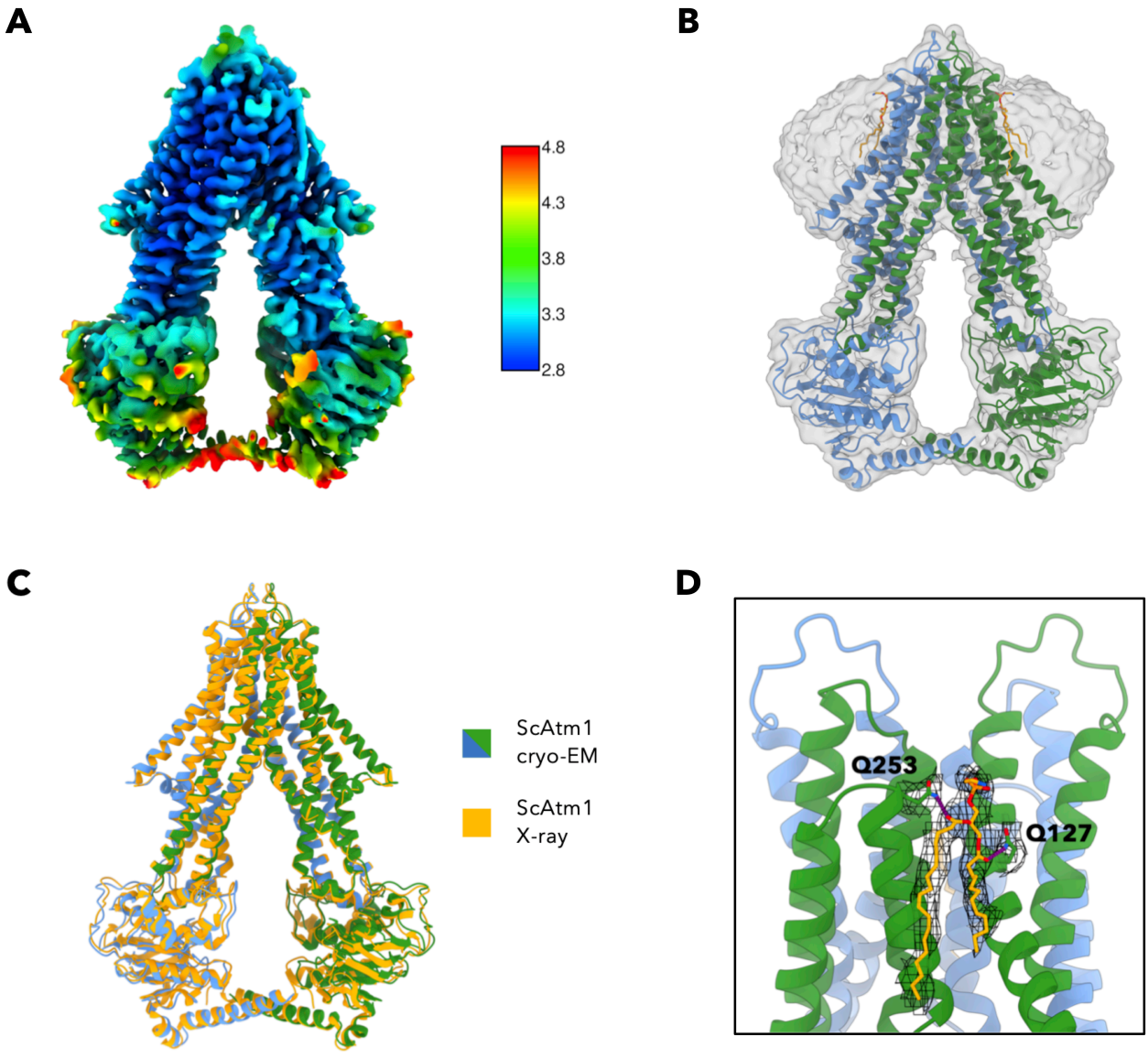

Figure S4: **Cryo-EM structure of nucleotide-free Atm1.** (**A**) Local resolution of cryo-EM map from 2.8 Å (blue) to 4.8 Å (red). (**B**) Atomic model (colour code as in Fig. 1) in the unsharpened cryo-EM map (transparent grey). (**C**) Superposition of cryo-EM (blue, green) and X-ray (orange; PDB ID: 4myc) structures of apo-Atm1 indicate close similarity. (**D**) Bound phospholipid molecule (orange) next to TM helices 1 and 3, in contact with Q127 (TM helix 1) and Q253 (TM helix 3; hydrogen bonds, purple dotted lines). Black mesh, density for lipid and sidechains Q127 and Q253. Rotated by 55° with respect to **B**.

Figure S5

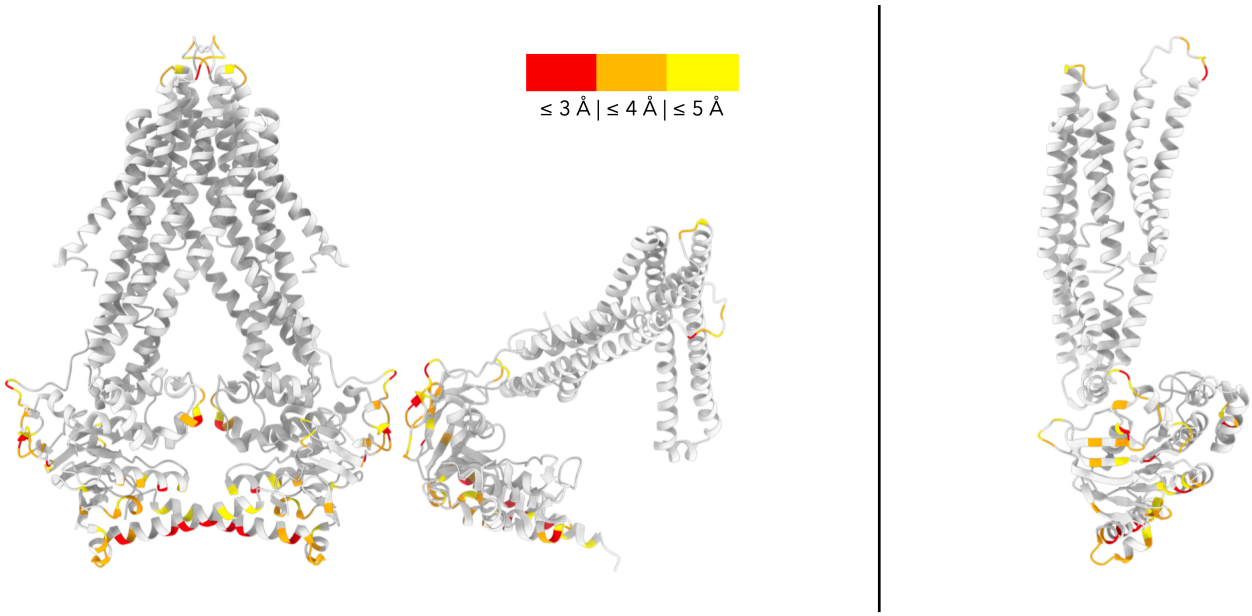

Figure S5: **Crystal contacts in the nucleotide-free X-ray structure of Atm1.** In the X-ray structure (PDB ID: 4myc), the crystal contacts are mostly confined to the NBDs and the loops connecting TM helices. Residues with nearest-neighbour distances ≤ 5 Å are coloured red (closest) to yellow. *Left*: Entire asymmetric unit. *Right*: One chain with the NBD interface pointing away from the viewer.

Figure S6

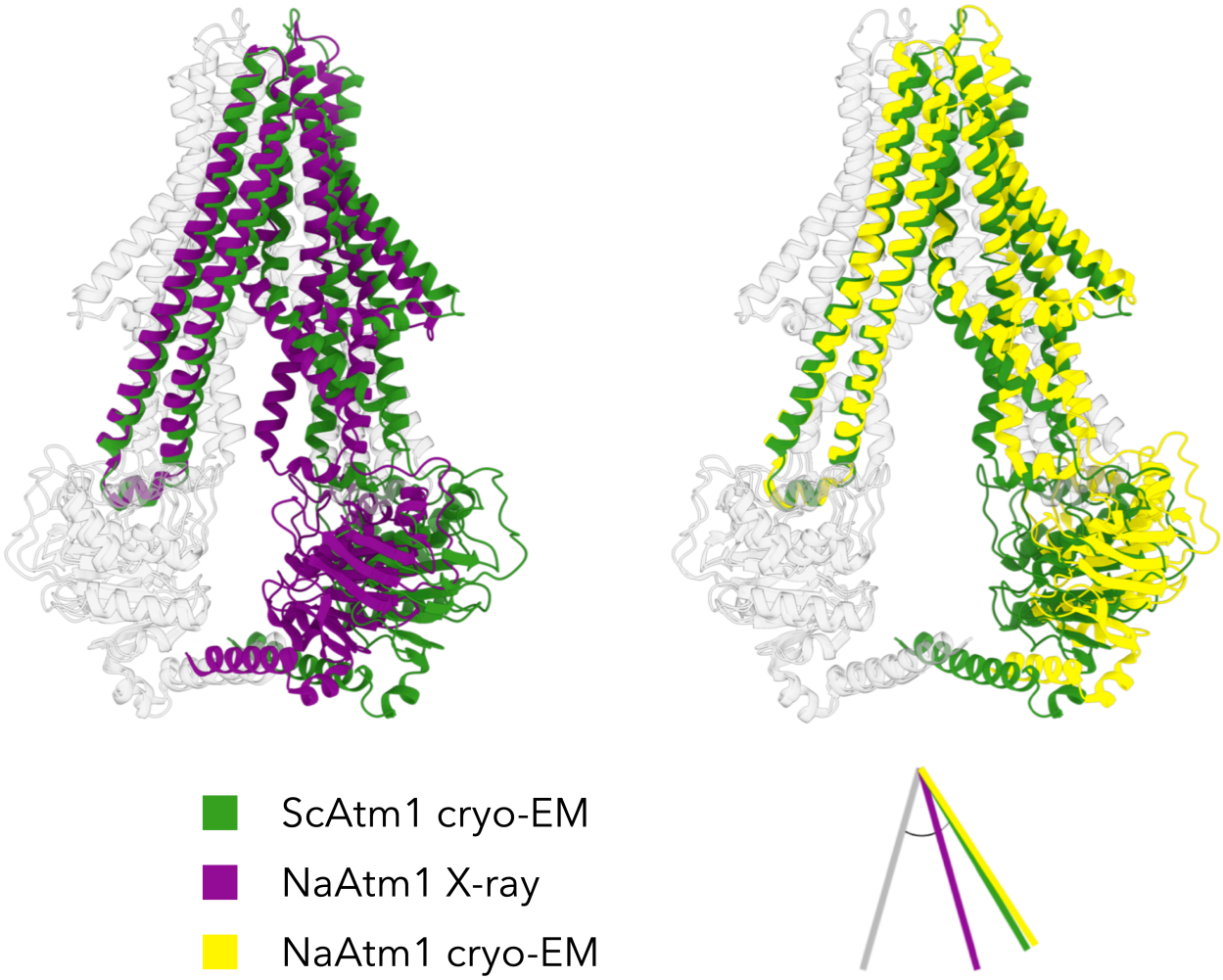

Figure S6: **Superpositions of nucleotide-free Atm1.** Cryo-EM structure of yeast Atm1 superimposed on crystal and cryo-EM structures of Atm1 from *N. aromaticivorans*. Chains used for alignment in translucent grey, indicating NBD separation increasing from the NaAtm1 crystal structure (left; other monomer in purple, PDB ID: 4mrn) to our yeast Atm1 cryo-EM structure (left and right; green), and to the NaAtm1 cryo-EM structure (right; yellow, PDB ID: 6vqu). The approximate angles between TM helices 4 of both monomers measured in the projected views are 33°, 46° and 49° (NaAtm1 crystal structure, ScAtm1 cryo-EM structure, NaAtm1 cryo-EM structure; as indicated on the lower right).

Figure S7

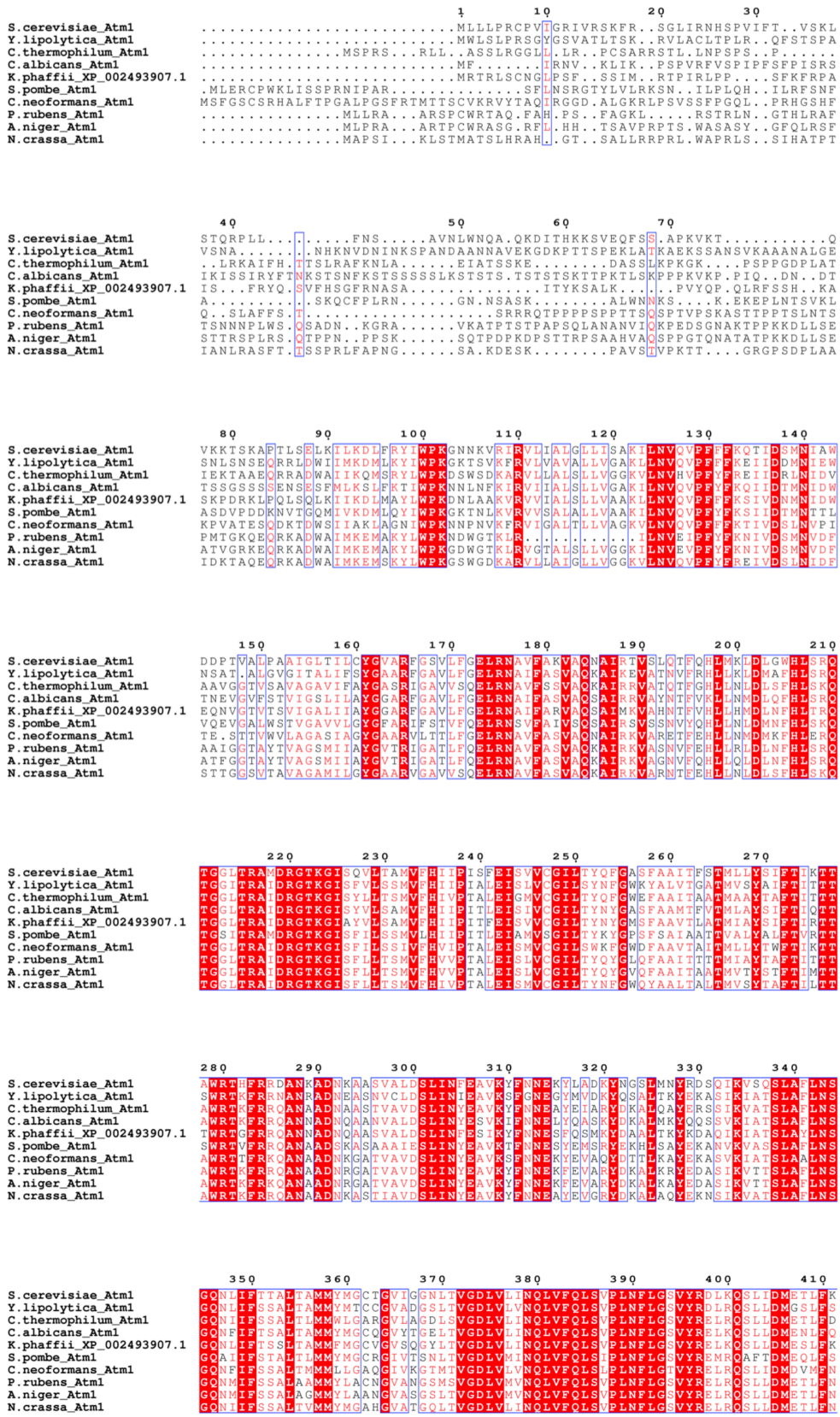
S.cerevisiae_Atm1
Y.lipolytica_Atm1
C.thermophilum_Atm1
C.albicans_Atm1
K.phaffii_XP_002493907.1
S.pombe_Atm1
C.neoformans_Atm1
P.rubens_Atm1
A.niger_Atm1
N.crassa_Atm1

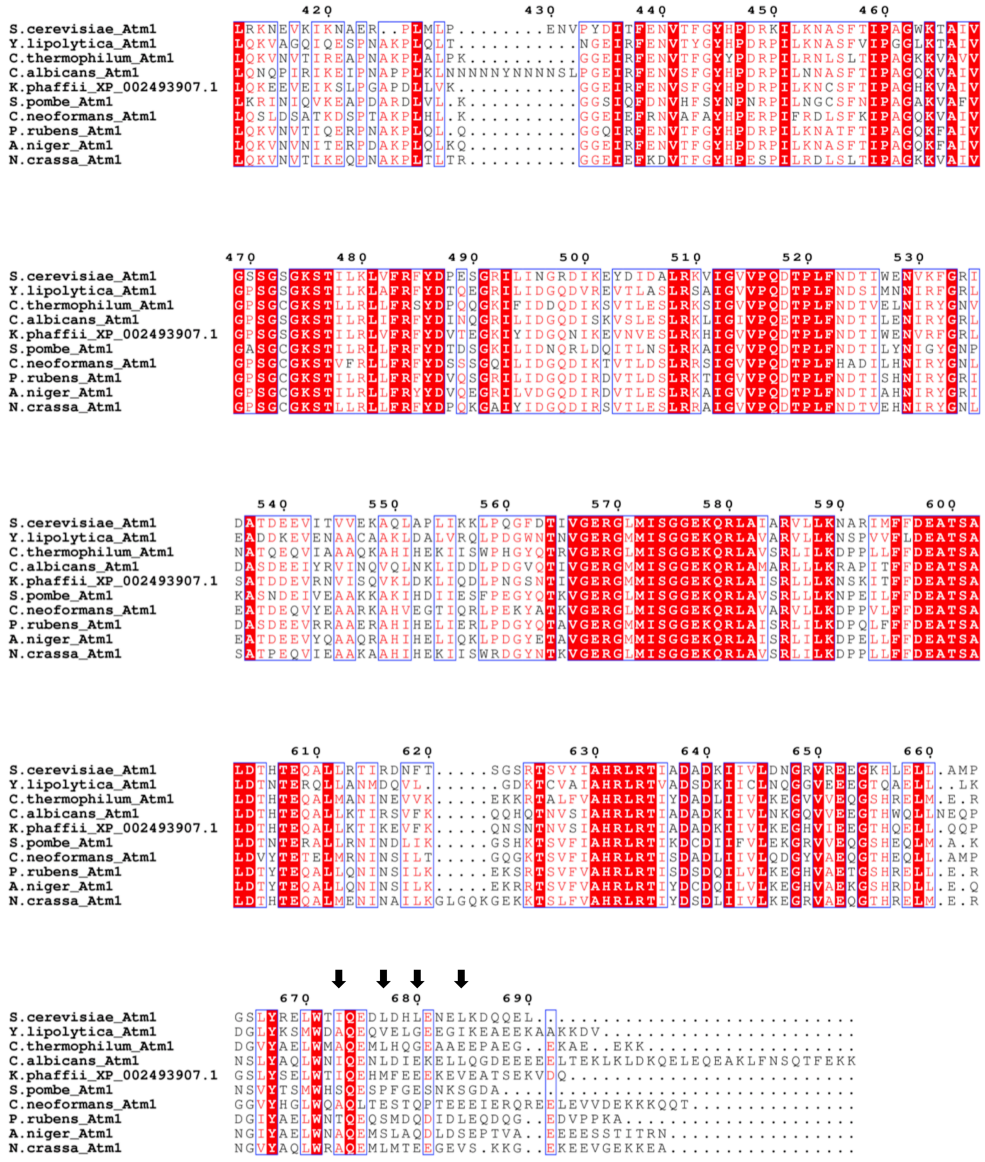

Figure S7: **Sequence alignment of fungal Atm1 homologues.** Numbering as for yeast Atm1. The salt bridge between R634 and E675 is conserved in fungi, while the hydrophobic patch on the C-terminal helices is found only in *S. cerevisiae* (I673, L677, L680 and L684; black arrows). Organisms shown are *Saccharomyces cerevisiae*, *Yarrowia lipolytica*, *Chaetomium thermophilum*, *Candida albicans*, *Komagataella phaffii*, *Schizosaccharomyces pombe*, *Cryptococcus neoformans*, *Penicillium rubens*, *Aspergillus niger* and *Neurospora crassa*.

Figure S8

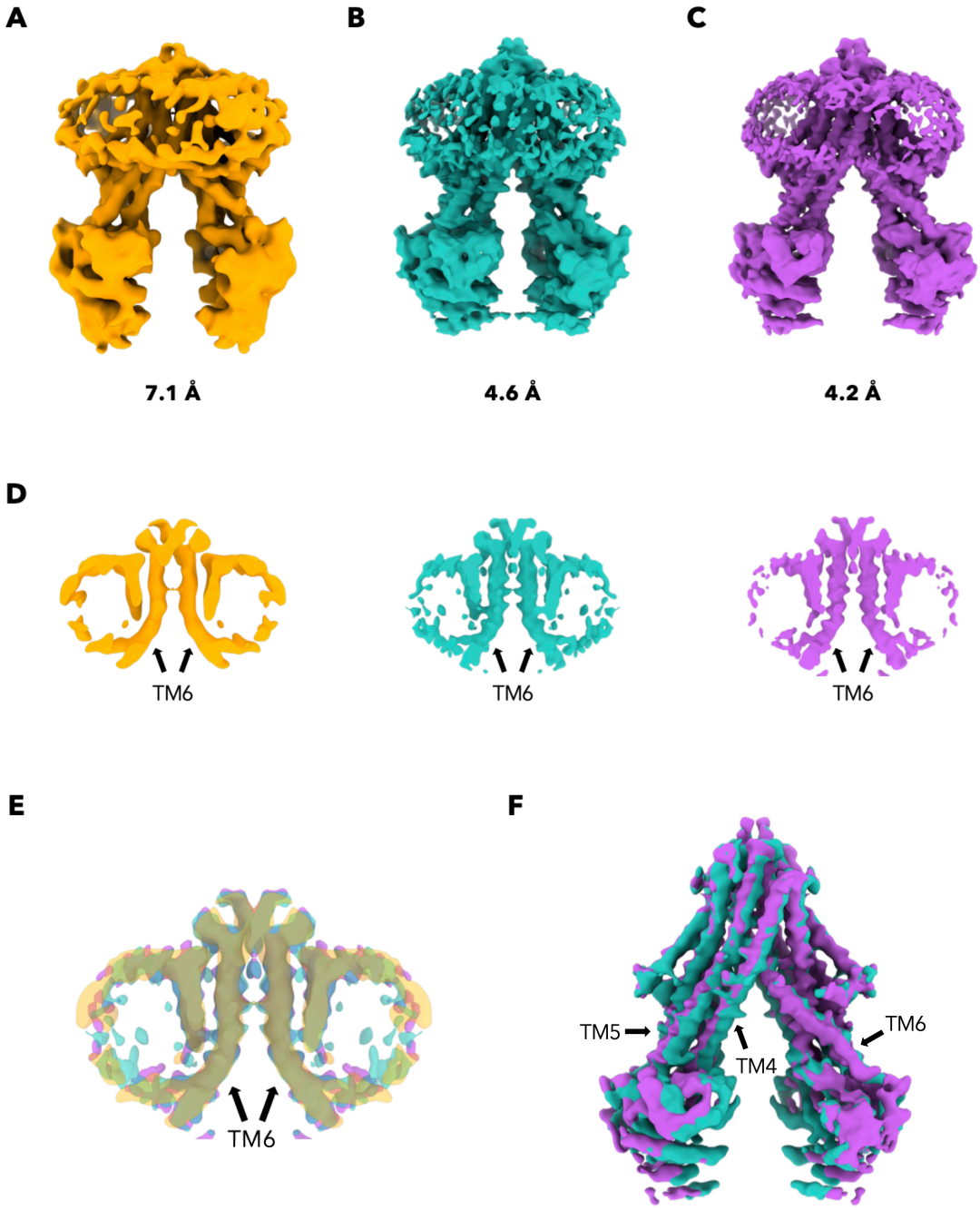

Figure S8: **Cryo-EM maps of nucleotide-free *Chaetomium thermophilum* Atm1 in MSP1E3D1 nanodiscs**. Sharpened maps after cryoSPARC Non-uniform refinements of the three classes in the 182,901 particle dataset reveal conformational heterogeneity with respect to NBD separation (**A**-**C**). For each class, the attained resolution is given. Classes with intermediate (orange, **A**), closer (turquoise, **B**) or wider NBD separation (violet, **C**) are shown. (**D**) Slices through TM regions of maps **A**-**C** (rotated by

60°) indicating the TM helices 6 (black arrows). (**E**) Superposition of the three map sections in **D** indicates that different NBD distances are not associated with significant differences in TM helix 6 position near the putative substrate-binding cavity. (**F**) A superposition of **B** and **C** (density threshold increased compared to **B** and **C**) indicates significant changes in the positions of TM helices 4 and 5 (black arrows). TM4, TM5, TM6, transmembrane helices 4, 5 and 6.

Figure S9

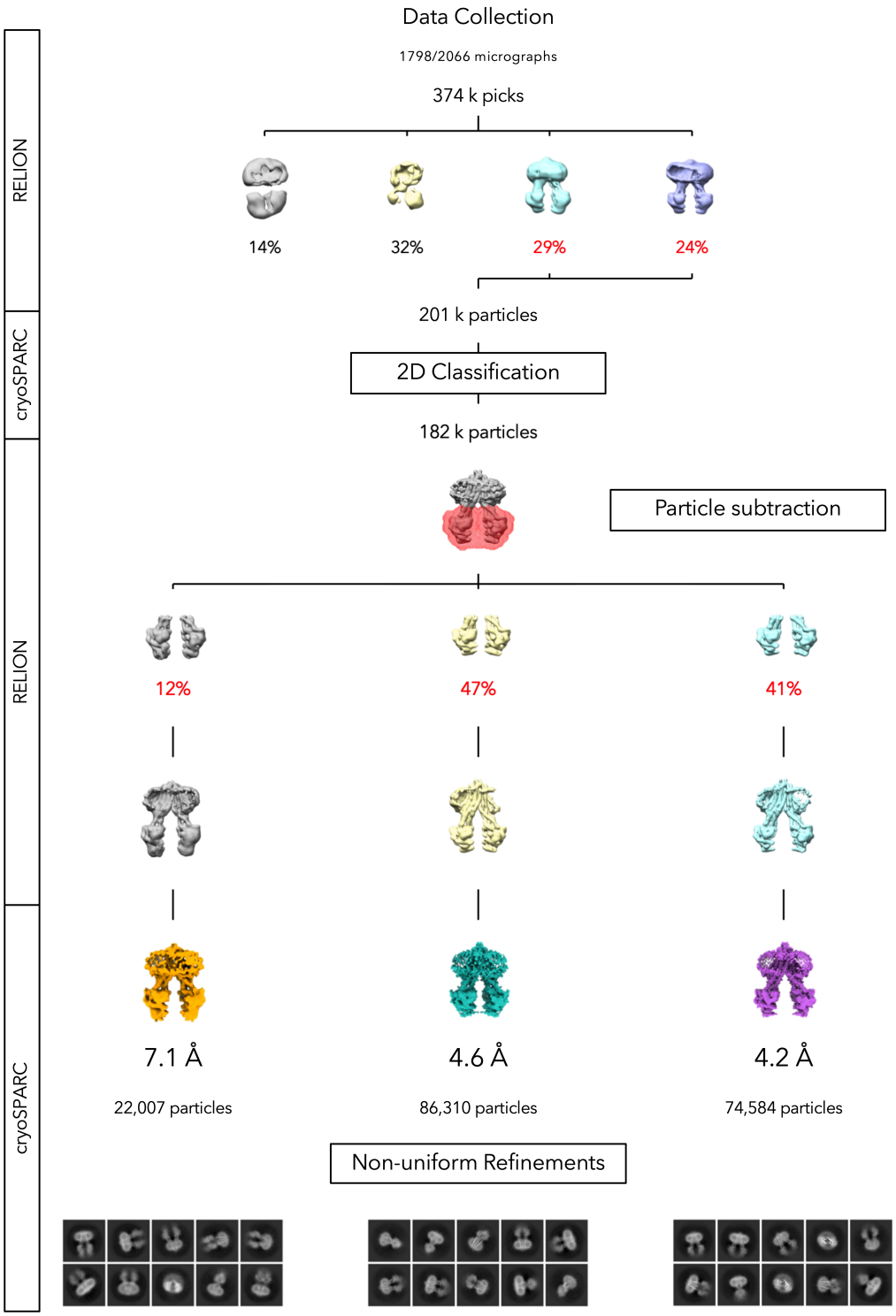

Figure S9: **Cryo-EM data processing pipeline for nucleotide-free *Chaetomium thermophilum* Atm1 in MSP1E3D1 nanodiscs.** See Methods.

Figure S10

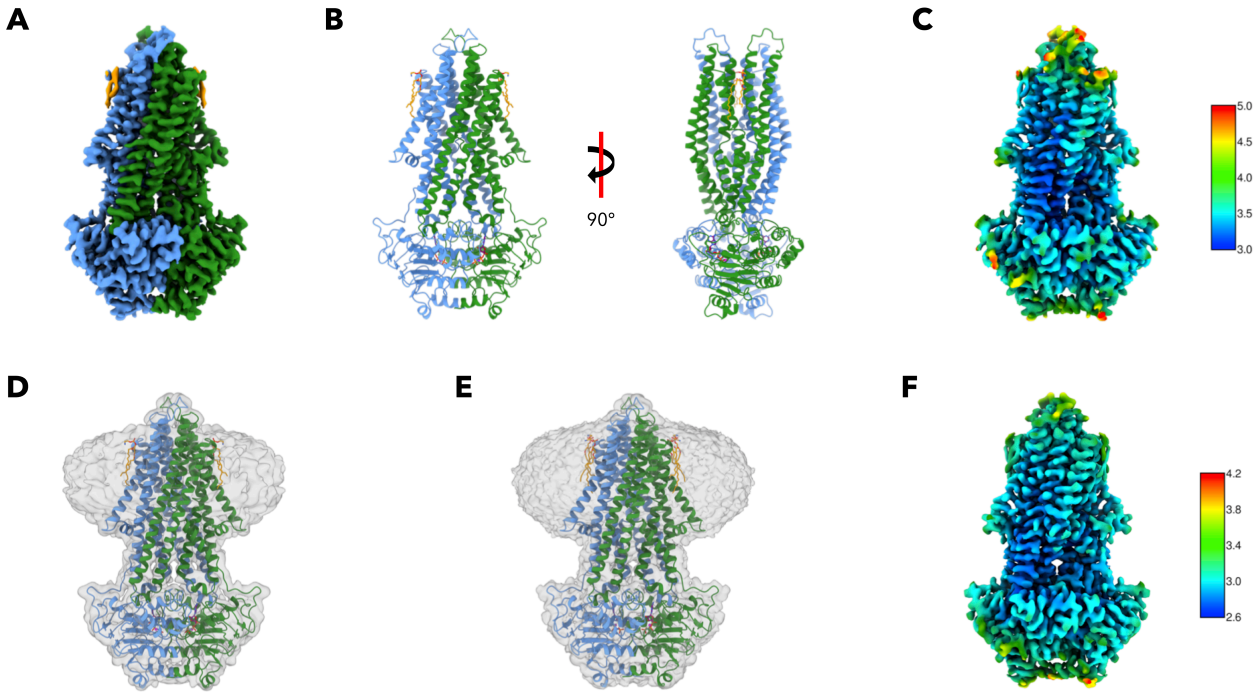

Figure S10: **Cryo-EM structures of AMP-PNP-Mg^{2+}-bound Atm1 in MSP1D1 and MSP1E3D1 lipid nanodiscs.** (**A** and **B**) The 3.4 Å cryo-EM map and model of AMP-PNP-Mg^{2+}-bound yeast Atm1 in MSP1D1 nanodiscs closely resemble that of Atm1 in the larger MSP1E3D1 nanodisc (colour coding as in Fig. 2A-B). (**C**) Local resolution of AMP-PNP-Mg^{2+}-bound Atm1 in MSP1D1 nanodiscs, 3.0 Å (blue) to 5.0 Å (red). (**D** and **E**) Atomic models (colour coding as in **B**) in the unsharpened cryo-EM maps (transparent grey). (**F**) Local resolution of MSP1E3D1 map as in **C**, from 2.6 Å (blue) to 4.2 Å (red).

Figure S11

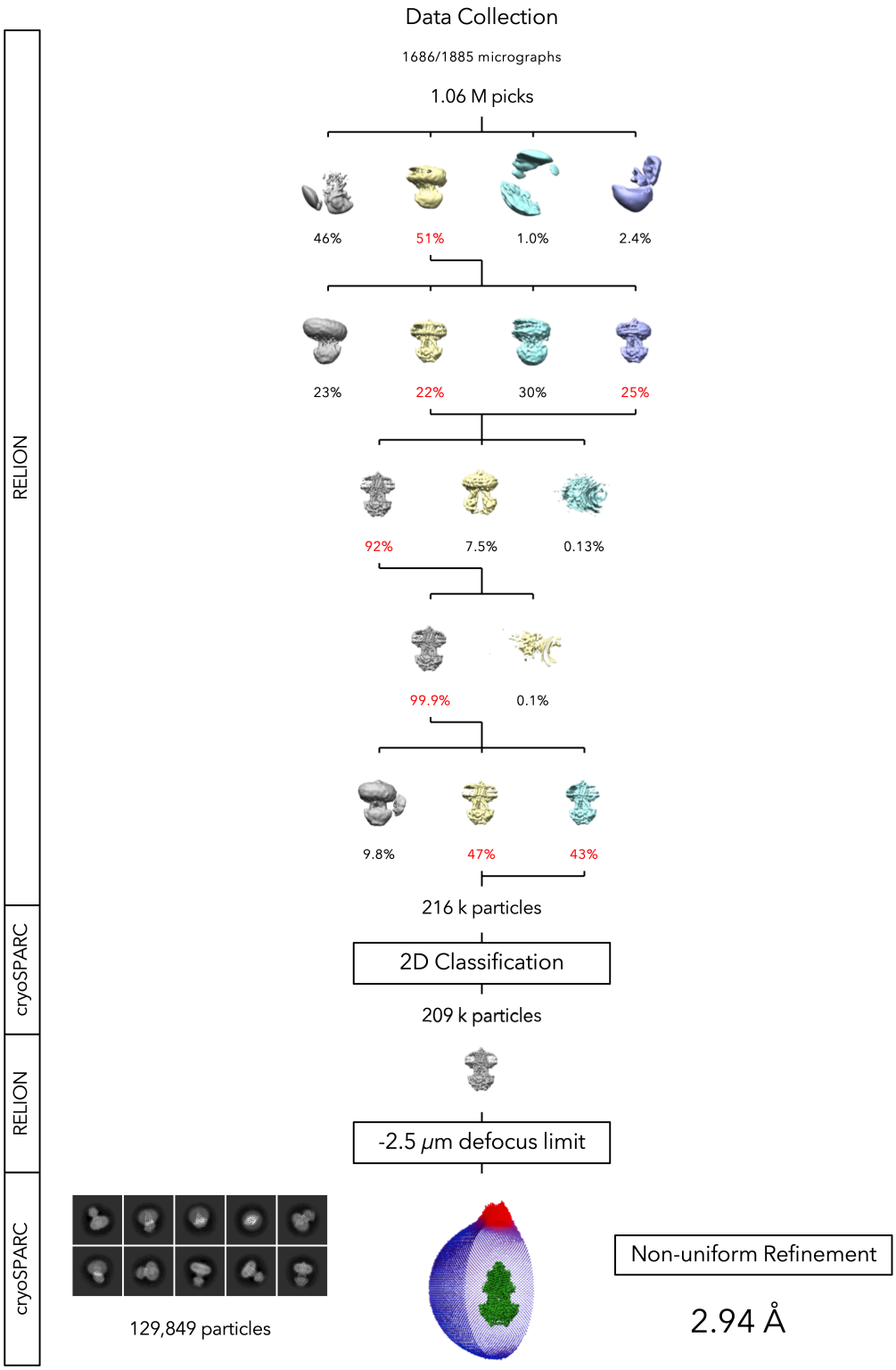

Figure S11: **Cryo-EM data processing pipeline of AMP-PNP-Mg^{2+}-bound yeast Atm1 in MSP1E3D1 nanodiscs.** See Methods.

Figure S12

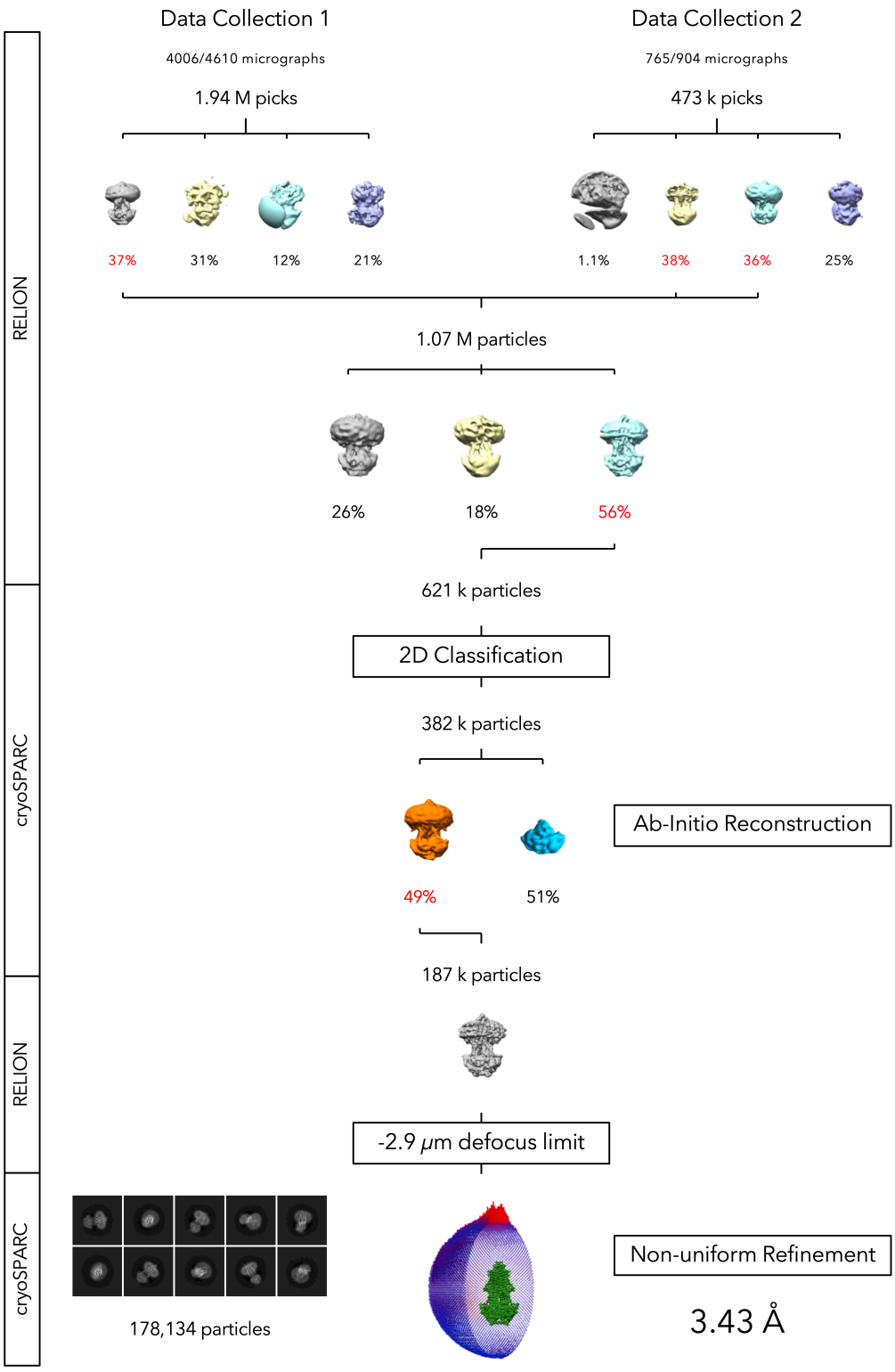

Figure S12: **Cryo-EM data processing pipeline of AMP-PNP-Mg^{2+}-bound yeast Atm1 in MSP1D1 nanodiscs.** See Methods.

Figure S13

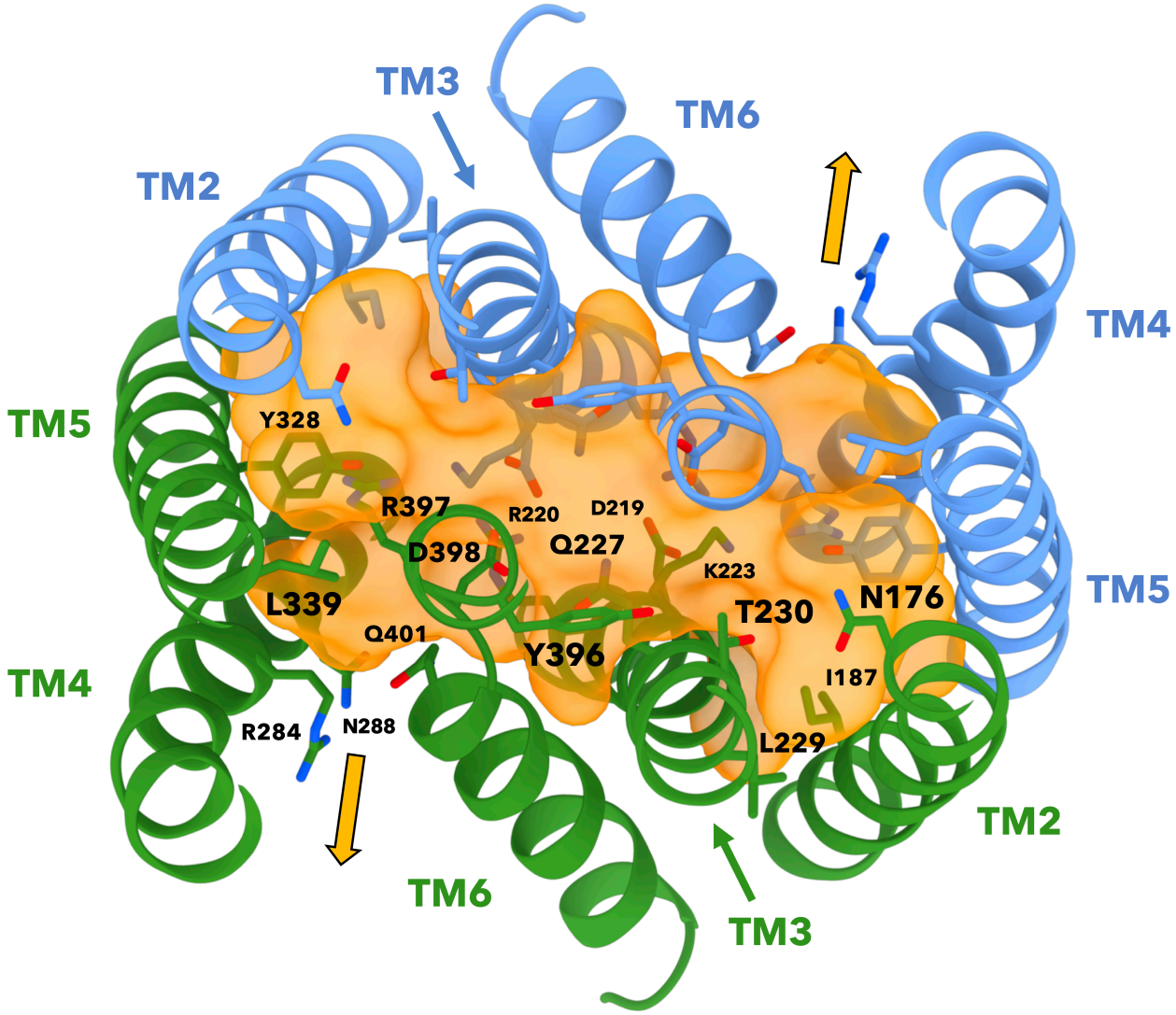

Figure S13: **Charged and polar sidechains of TM helices 2 to 6 define a cavity within AMP-PNP-Mg^{2+}-bound Atm1.** Slice through the AMP-PNP-Mg^{2+}-bound Atm1 structure in MSP1E3D1 lipid nanodiscs (colour code as in Fig. 2C; cavity, translucent orange volume; structure rotated by 25° with respect to Fig. 2C (right)). TM helices 2 to 6 are labelled. TM helix 1 and the N-terminal elbow helix are omitted for clarity. Sidechains of selected residues outlining the cavity are labelled for the green protomer only. Label font size of amino acid residues decreases with increasing distance from the viewer. Residues Y396 to D398 are located in the kink of TM helix 6. Orange arrows mark the narrow channels towards the mitochondrial matrix.

Figure S14

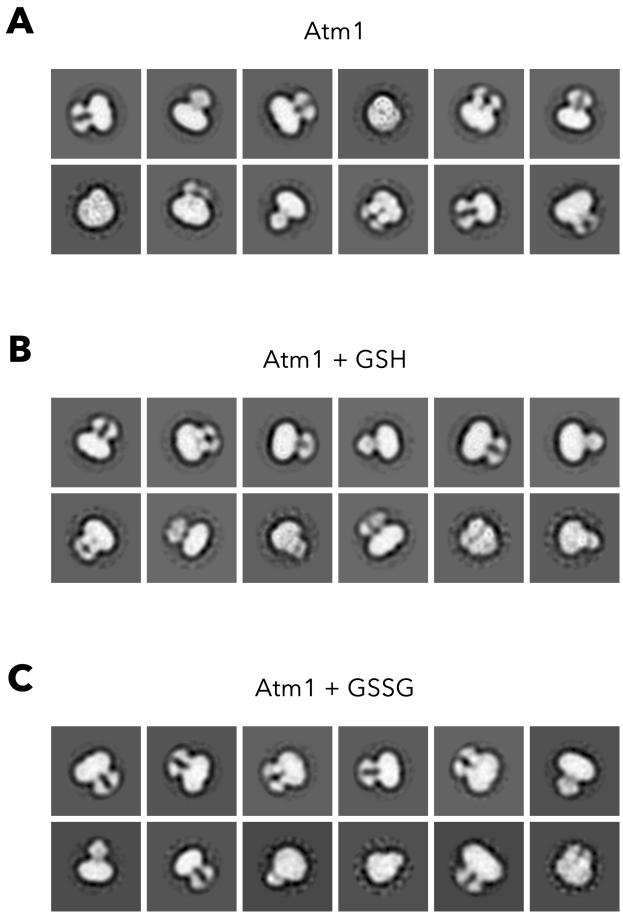

Figure S14: **Addition of glutathione to Atm1 does not cause NBDs to associate.** Negative-stain EM 2D class averages of Atm1 in MSP1D1 lipid nanodiscs (**A**) without added potential substrates, and with 2 mmol/l GSH (**B**) or GSSG (**C**), each representing a 6,000-fold molar excess over Atm1 dimers. The class averages shown represent 97% (apo), 83% (GSH) and 98% (GSSG) of all particles.

Figure S15

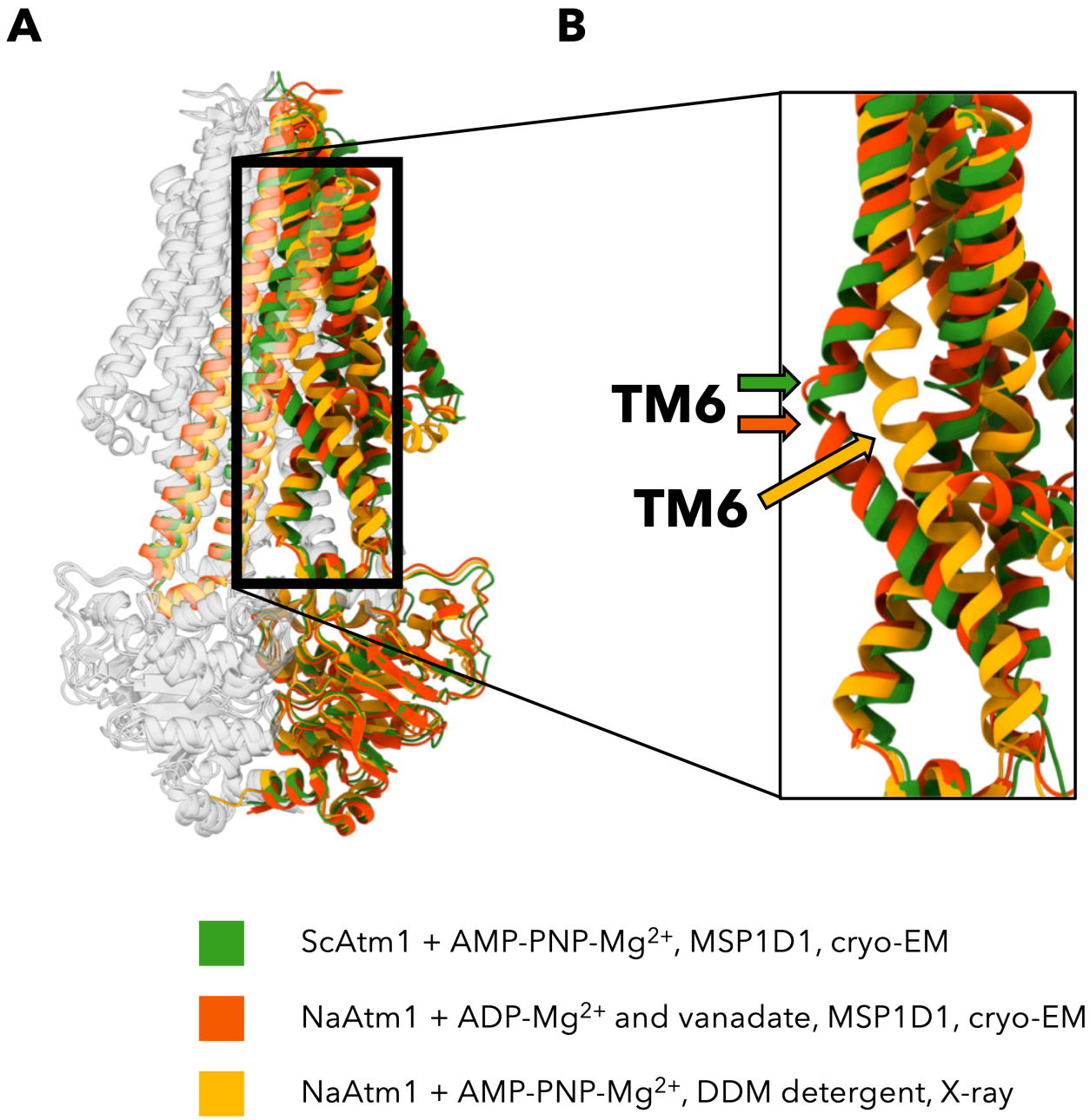

Figure S15: **Superposition of Atm1 protomers.** (**A**) Comparison of cryo-EM structures of AMP-PNP-bound yeast Atm1 (green, MSP1D1 nanodisc), ADP-bound NaAtm1 in MSP1D1 nanodiscs (dark orange; PDB ID: 6par), and the X-ray structure of AMP-PNP-bound NaAtm1 in DDM (light orange; PDB ID: 6vqt). (**B**) The inset reveals differences in the TM helix 6 hinge region (coloured arrows). TM helices 4 and 5 were omitted for clarity.

Figure S16

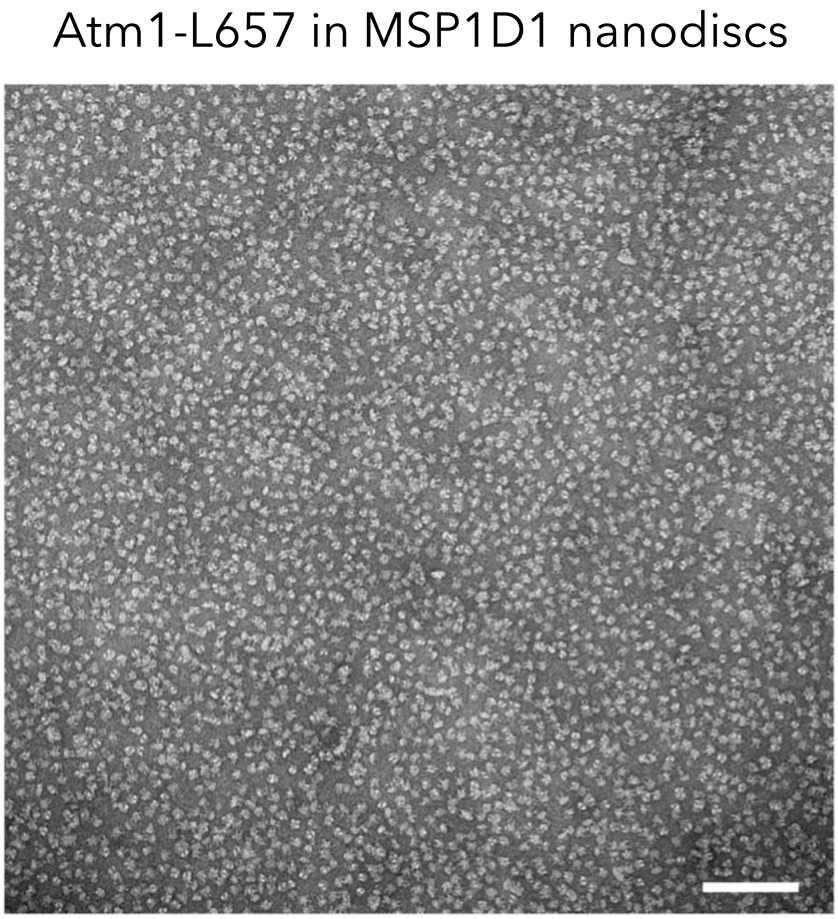

Figure S16: **Negative-stain EM of Atm1-L657 in MSP1D1 lipid nanodiscs.** Micrograph of the truncation mutant Atm1-L657 reconstituted into MSP1D1 nanodiscs (scale bar 100 nm). The purified and concentrated reconstitution sample (0.02 mg/ml) was not diluted for negative-stain EM.

Figure S17

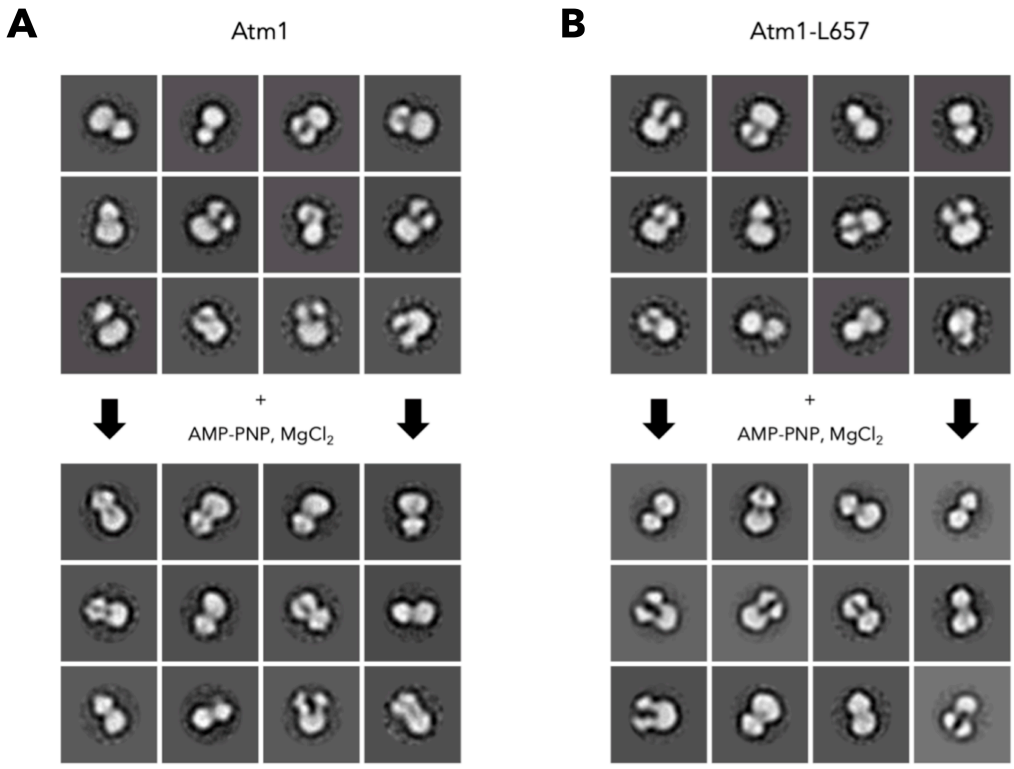

Figure S17: **NBD separation and AMP-PNP-Mg^{2+}-induced NBD association of wild-type Atm1 and Atm1-L657 do not depend on the C-terminal helices and nanodisc scaffolds.** (**A** and **B**) Negative-stain 2D class averages of Atm1 and Atm1-L657 in DDM detergent indicate the absence of wide-open apo states and show that the C-terminal helices are not needed for NBD closure.

Table S1

	Atm1 apo (MSP1D1); EMDB 13613, PDB 7psl	**Atm1 – AMP-PNP-Mg^{2+} (MSP1D1);** EMDB 13614, PDB 7psm	**Atm1 – AMP-PNP-Mg^{2+} (MSP1E3D1);** EMDB 13615, PDB 7psn	**CtAtm1 apo (MSP1E3D1, class 1)** EMDB 13616	**CtAtm1 apo (MSP1E3D1, class 2)** EMDB 13617	**CtAtm1 apo (MSP1E3D1, class 3)** EMDB 13618
Data collection and processing						
Microscope	Titan Krios G3i	Titan Krios G3i	Titan Krios G2	Titan Krios G3i		
Detector	K3	Falcon III	K2 Summit	K3		
Magnification	105,000	96,000	165,000	105,000		
Voltage [kV]	300	300	300	300		
Electron exposure [$e^-/Å^2$]	64	50	68	63		
Defocus range [μm]	-1.2 – -3.5	-1.0 – -3.5	-0.9 – -3.6	-1.0 – -4.0		
Pixel size [Å]	0.837	0.833	0.828	0.837		
Initial particle images [no.]	3,008,035	2,414,998	1,063,341	374,012		
Final particle images [no.]	439,015	178,134	129,849	22,007	86,310	74,584
Symmetry imposed	C2	C2	C2	C2	C2	C2
Map resolution [Å]	3.3	3.4	2.9	7.1	4.6	4.2
FSC threshold	0.143	0.143	0.143	0.143	0.143	0.143
Refinement						
Initial model used	-	-	-	-	-	-
Map sharpening *B* factor [$Å^2$]	-141	-154	-106	-607	-291	-217
Model composition						
Non-hydrogen atoms	9512	9244	9244	-	-	-
Protein residues	1200	1170	1170	-	-	-
Ligands	2 PO4, 2 LOP	2 ANP, 2 MG, 2 LOP	2 ANP, 2 MG, 4 LOP	-	-	-
B factors [$Å^2$]						
Protein	91.2	95.9	87.5	-	-	-
Ligand	78.6	107.0	96.2	-	-	-
R.m.s. deviations						
Bond lengths [Å]	0.006	0.005	0.007	-	-	-
Bond angles [°]	0.538	0.814	0.657	-	-	-
Validation						
MolProbity score	1.59	1.43	1.39	-	-	-
Clashscore	5.9	3.94	5.05	-	-	-
Poor rotamers [%]	0.0	0.0	0.0	-	-	-
Ramachandran plot						
Favored [%]	96.1	96.3	97.3	-	-	-
Allowed [%]	3.9	3.7	2.7	-	-	-
Disallowed [%]	0.0	0.0	0.0	-	-	-

Table S1: **Data collection and processing parameters, and model statistics.**